Article

Optimization Analysis of the Arrangement of the Submerged Floating Tunnel Subjected to Waves

Wenbo Pan [1], Cheng Cui [1,*], Chun Chen [1,*], Mingxiao Xie [1], Qian Gu [2] and Zhiwen Yang [1]

1   National Engineering Research Center of Port Hydraulic Construction Technology, Tianjin Research Institute for Water Transport Engineering, M.O.T., Tianjin 300456, China; panofficial@163.com (W.P.); crabsaver@163.com (M.X.); oyangzhiwen@126.com (Z.Y.)
2   State Key Laboratory of Coastal and Offshore Engineering, Dalian University of Technology, Dalian 116024, China; gqian@dlut.edu.cn
*   Correspondence: chengcui1984@163.com (C.C.); chenchun9999@163.com (C.C.); Tel.: 86-188-9228-3383 (Cheng Cui)

Abstract: The motion responses, mooring tensions, and submergence depth are the dominant factors for the arrangement of the Submerged Floating Tunnel (SFT) subjected to waves. Generally, the maximum values of motion responses, mooring tensions, and absolute submergence depth are mainly focused on. In the present study, experiments are implemented to measure the motion responses and mooring tensions of the SFT with different mooring patterns and submergence depths under waves with different characteristic wave heights and periods. In order to evaluate the arrangement of the SFT more effectively and comprehensively, besides the maximum values, several new characteristic parameters are introduced. Such parameters account for the motion responses in the frequency domain, the uniformity of the tension distribution, the length of time during which the cable reaches a relaxed condition during wave action, the KC number, the dimensionless period, the wave height, and the submergence depth. The results from the optimization analysis show the following: according to the characteristic values of motion responses and mooring tensions, the pattern of diagonal cables is better than that of diagonal cables + vertical cables; and within the range of the present experiments, there are optimal dimensionless parameters—the dimensionless submergence depth $d_0/L_P \geq 0.15$, the KC number ≤ 0.8, or the dimensionless wave height $Hs/d_0 \leq 0.10$—for the condition of which the dynamic responses and mooring tensions vary slightly.

Keywords: submerged floating tunnel (SFT); relative submergence depth; KC number; mooring pattern; motion response; tension

1. Introduction

The Submerged Floating Tunnel (SFT) is a new type of cross-water transportation structure that mainly consists of tunnel tubes, constrained along the tunnel and at the ends. Equilibrium is established by the gravity and buoyancy of the tunnel tube and mooring tension of the restraints [1–3]. Based on the different restraints along the tunnel, the SFT can be classified as a fixed-support tunnel, floating-tube tunnel, and anchor-cable tunnel. The anchor-cable tunnel has shown a better overall performance as compared with the fixed-support tunnel and floating-tube tunnel. This type of SFT has been the primary focus of researchers and is the most commonly produced structural form.

With respect to the mooring pattern of the SFT, the mooring system plays an important role in the motion responses of the floating structures subjected to waves, while the majority of the tension in the mooring is connected to the wave actions [4]. Seo et al. [5] experimentally studied the dynamic response of an SFT under regular waves and discussed the effect of the mooring pattern. The test results show that the single vertical moored SFT oscillates severely, while the w-type double-moored SFT oscillates slightly. Cifuentes et al. [6] numerically simulated the dynamic response of an SFT under regular waves. The

vertical and inclined mooring systems were compared to find a better design to limit SFT movement and minimize mooring tension. The results show that the inclined mooring system is more effective in restricting SFT movement compared to the vertical mooring system. Jeong et al. [7] analyzed the feasibility of the SFT with a mooring system combining vertical and inclined tethers by using the finite element program ABAQUS-AQUA and pointed out that it could be effectively applied when the spacing is less than 40.0 m and the inclination angle is 45.0 degrees. Lee et al. [8] used numerical software OrcaFlex and CHARM3D to simulate the dynamic responses of two types of SFTs under the waves and seismic excitations in the time domain. The dynamic responses of the short-rigid-free-end SFT with vertical and inclined mooring systems were investigated. The results show that mooring tension increases in the inclined mooring system under horizontal earthquakes, while for vertical earthquakes, there is an increase in mooring tension in both the inclined and vertical mooring systems. Especially, when the seismic frequency is close to the natural frequency of the SFT, it is much more dangerous. Muhammad et al. [9] numerically investigated the motion responses and internal forces of the SFT under hydrodynamic and three-dimensional seismic excitations to test the overall performance of the SFT. The dynamic responses of the SFTs with three different mooring systems were evaluated to compare the stability of different mooring configurations. The results show that the moored SFT with a combination of tension legs and single inclined mooring cables is effective under moderate environmental conditions. Under harsh environmental conditions, the SFT should be moored by a combination of tension legs and double inclined mooring cables or only by double inclined mooring cables. Jin et al. [10] used the time-domain numerical software OrcaFlex to simulate the dynamic responses of a 1000 m long circular SFT with both ends fixed under irregular waves. The vertical mooring system (VM) and inclined mooring system (IM) were compared to investigate their overall performances. The results show that the horizontal response of VM is larger than that of IM due to the smaller horizontal stiffness and its lowest natural frequency closer to the incident wave frequency. The vertical response of VM is mainly downward and is also affected by set-down. The bouncing tension of the mooring line increases sharply when the SFT bounces back from the slack mooring condition caused by large vertical downward motion. Won et al. [11] numerically simulated the dynamic responses of the SFT with a dual section. Two types of dual-SFTs were proposed according to the mooring system, and the analysis results of hydrodynamic characteristics show that as the wave steepness increases, the sway of the SFT increases significantly, while the increase in heave is smaller, and that for inclined mooring system, a relaxation phenomenon lowering from the initial position occurs when the steepness of the wave is 0.028 and the motion increases rapidly. Wu et al. [12] proposed a new SFT consisting of three circular section tubes and a fiber-reinforced plastic (FRP) rigid truss structure. In addition, a series of model tests were carried out under wave-flow conditions to investigate the anti-vibration performance of the SFT. The results show that compared with other models, the free vibration frequency of each degree of freedom for the proposed SFT is much lower, which can avoid the resonance with the wave frequency and ensure the safety of the structure. The proposed SFT has better anti-vibration performance under different external loads, especially in the roll motion component. The mooring system of the proposed SFT has a smaller mooring tension which is below the limits' value.

For the submergence depth of the SFT, Cifuentes et al. [6] numerically simulated the dynamic response of the SFT under regular waves. The results show that both the motion response and mooring tension increase with the wave height and period and decrease with submergence depth due to the reduced wave action. The inclined mooring system restricts the motion response more effectively than the vertical mooring system with the same submergence depth. Won et al. [13] used the nonlinear finite element code ABAQUS–AQUA to investigate the dynamic response of a new type of SFT under the irregular wave. The dynamic responses, including the motion response, internal force, and fatigue damage, under severe waves were systematically investigated. The results show that the dynamic response of the SFT can be effectively controlled by designing a

"suitable" submergence depth. It results from the wave force reduction caused by the deep draft design. Chen et al. [14] proposed a theoretical method to investigate the nonlinear dynamic response of the SFT mooring system under the combined action of parametric excitation and hydrodynamic excitations (i.e., wave- and vortex-induced loading). Based on the Hamilton principle, the governing equations of the SFT system considering the coupled degrees of freedom and mooring cables are established and solved. The results show that the motion amplitude of the mooring cables and the tube decreases with the increase in the submergence depth. When the submergence depth is within the range of 5~40 m, the motion amplitude reduction rate of the mooring cable is greater than that of the tube. When the submergence depth is more than 40 m, the motion response of the tube will decrease more significantly. Deng et al. [15] experimentally investigated the drag force on a double-tube SFT with different Reynolds numbers and submergence depths using a simplified rigidly connected tandem twin-cylinder model under strong current. The results show that both the vortex-induced vibration response and mean drag coefficient decrease with the decrease in the submerged depth, especially when the depth ratio $h^* < 3.7$ ($h^* = h/D$, where h is the distance from the bottom of the SFT to the initial free surface and D is the outer diameter of the SFT). Yang et al. [16] experimentally investigated the 2D motion characteristics of the SFT under regular waves. The experimental phenomena of SFT motion during the interaction between the SFT and waves are described in detail. The effect of experimental parameters, including the wave height, wave period, submergence depth, buoyancy-to-weight ratio (BWR), and mooring line angle, are thoroughly analyzed. The results indicate that as the submergence depth increases, the amplitude of the motion characteristics decreases significantly. For the SFT moored under the water surface, the motion response of sway, heave, and roll is much smaller than those of the SFT located on the water surface. Chen et al. [17] numerically investigated the effects of wave height, wave period, submergence depth, and BWR on the nonlinear hydrodynamic characteristics of the wave–SFT interaction based on 49 designed cases. The results show that the maximum motion response and mooring tension increase with wave height and wave period and decrease with submergence depth. Won et al. [18] investigated the hydrodynamic characteristics of the SFT under regular and irregular waves by time-domain hydrodynamic analysis. The analysis results show that the dynamic response of the SFT can be effectively reduced by deep draft design.

The above studies show that the effects of the mooring pattern and submergence depth on the dynamic response of the SFT are critical. Previous studies on optimal mooring patterns for the SFT mainly refer to regular wave loads, the maximum motion response, and the mooring tension in the time domain. In addition, previous studies on the submergence depth of the SFT mostly focus on the absolute submergence depth of a floater. In engineering, submerged floating structures, such as the SFT, are subject to both "absolute" and "relative" submergence depth. The absolute submergence depth is established to guarantee a specific navigable depth, while the relative submergence depth is determined to reduce the surface-wave-induced dynamic response. Theoretically, the relative submergence depth can be defined by the ratio of the absolute submergence depth d_0 to the wavelength L_P, represented as d_0/L_P. The wavelength is influenced by two factors: the water depth and wave period. This implies that the impact of relative submergence depth on dynamic response is essential to the effect of the wave period. Moreover, the relationship between the significant wave height and absolute submergence depth (represented as H_S/d_0, which can be defined as the relative wave height), as well as the relationship between the natural period of the mooring system and wave period, are also important factors influencing the dynamic response of the SFT.

In the present study, it is experimentally investigated that the mooring pattern and submergence depth influence the dynamic responses of the SFT. Based on the motion response and mooring tension derived from the tests, the mooring pattern was examined comprehensively in terms of three factors: the maximum value and spectral area of the motion response, the maximum value and uniformity of the mooring tension, and the

length of time during which the cable reached a relaxed condition during wave action; moreover, the effects of submergence depth on the dynamic response of the SFT were investigated comprehensively in terms of four factors: the relative submergence depth, relative period, relative wave height, and KC number. Finally, the optimal mooring pattern and submergence depth for the SFT were determined.

2. Experiments

2.1. Experimental Equipment and Instruments

The model tests were carried out in a test tank at the State Key Laboratory of Coastal and Offshore Engineering, Dalian University of Technology. The test tank was 60.0 m long, 2.0 m wide, and 1.8 m deep. The wave generation system was a Hydro-servo random wave maker system, which can generate waves with periods ranging from 0.5 s to 5.0 s. At the end of the test tank, multiple layers of energy dissipation equipment were installed for effective wave dissipation.

The motion responses of the SFT were measured by a non-contact 6-degree-of-freedom measurement system, consisting of dual-CCD (charge-coupled device) cameras and a data acquisition system. Three light markers were arranged on a plane and fixed on top of the SFT model to record the six-degrees-of-freedom motion components by the dual-CCD cameras. The motions of the light markers were continuously measured by the dual-CCD cameras at 30 frames per second and the signals were processed to recover the instantaneous position of each marker in a calibrated coordinate system. The mooring tension was measured by the tension sensor with an accuracy of 0.1 N. The wave heights were measured by the DS30 wave measuring system, which controlled 64 wave gauges synchronously. The wave gauges were calibrated before tests with an accuracy of 0.1 mm.
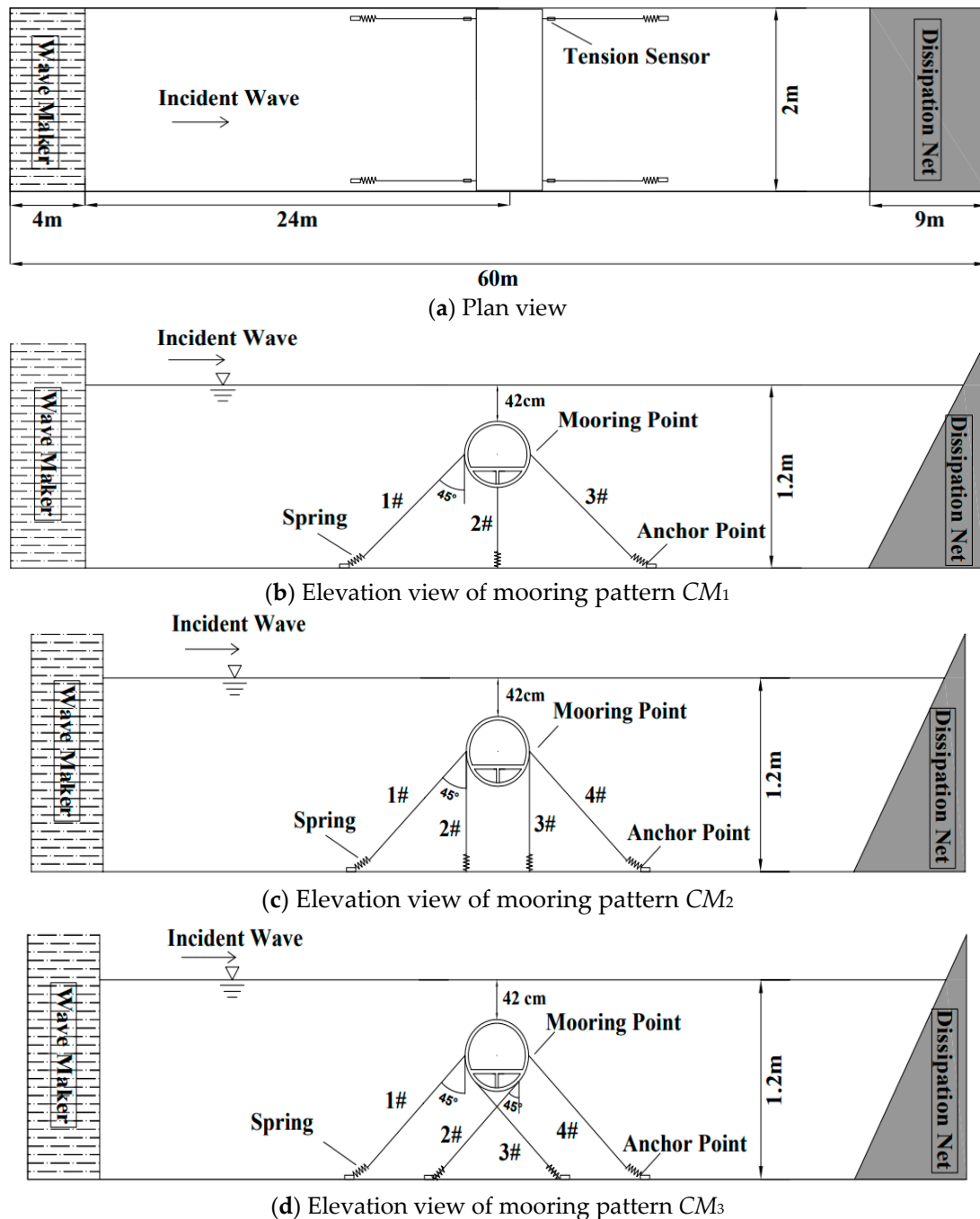
2.2. Model Parameters and Layout

The engineering background of the SFT in the test was the conceptual design of the SFT by the China Communications Construction SFT Technical Joint Research Team. The outer diameter of the SFT was 12 m and the interval between the mooring cables along the longitudinal direction of the tunnel was 120 m. It should be noted that the SFT was considerably long. In this study, a finite-length section (120 m) was intercepted and simplified into a rigid submerged horizontal cylinder for the two-dimensional experiment. The SFT model was made of organic glass. The model was designed in accordance with the Froude scaling law, and the geometric scale was determined as $\lambda = 60$ according to the test equipment conditions, the geometrical dimension of the model, and the boundary effect. The clump weights were placed to adjust the center of gravity (COG) and buoyancy weight ratio (BWR) of the SFT model. The length of the SFT model was designed to be 1.96 m according to geometric scale (the test tank width is 2.0 m) and six smooth universal balls were arranged on both ends of the SFT model to prevent the tunnel section from colliding with the flume side wall during the tests. The mechanical parameters of the prototype and model SFT are presented in Table 1.

Table 1. Geometric and hydrodynamic parameters of the SFT ($\lambda = 60$).

Parameters	Symbols	Prototype	Unit	Model	Unit
Length	B	120.0	m	200.0	cm
Diameter	D	12.0	m	20.0	cm
Mass	G	11,232	t	52.0	kg
Centre of gravity	b	9.6	m	16.0	cm
Centre of buoyancy	b_0	12.0	m	10.0	cm
Buoyancy weight ratio	BWR	1.20	-	1.20	-
Absolute submergence depth	d_0	25.2	m	42.0	cm

Three mooring patterns of the SFT were selected, which are hereafter denoted as C_{M1}, C_{M2}, and C_{M3} for convenience. The lower ends of the mooring lines were anchored to the bottom of the wave flume. The top ends together with tension sensors were connected to

the circular cross-section, and each connecting point was 20 cm measured from the edge of the horizontal cylinders. The plan views of the three mooring patterns are the same as those shown in Figure 1a. The number of cables as well as the angle and position of the mooring lines of each mooring pattern were different, as shown in Figure 1b–d. The specific setups of the three mooring patterns are briefly described as follows:

(**a**) Plan view

(**b**) Elevation view of mooring pattern CM_1

(**c**) Elevation view of mooring pattern CM_2

(**d**) Elevation view of mooring pattern CM_3

Figure 1. Sketch of the three types of mooring patterns.

Mooring pattern C_{M1}: There are three cables at either end of the horizontal cylinder, two cables are diagonal and one cable is vertical, where the diagonal cables are at 45° to the vertical, as shown in Figure 1b. The system is in equilibrium when the initial tension of each cable is F_0 = 17 N.

Mooring pattern C_{M2}: There are four cables at either end of the horizontal cylinder, two cables are diagonal and two cables are vertical, where the diagonal cables are at 45° to
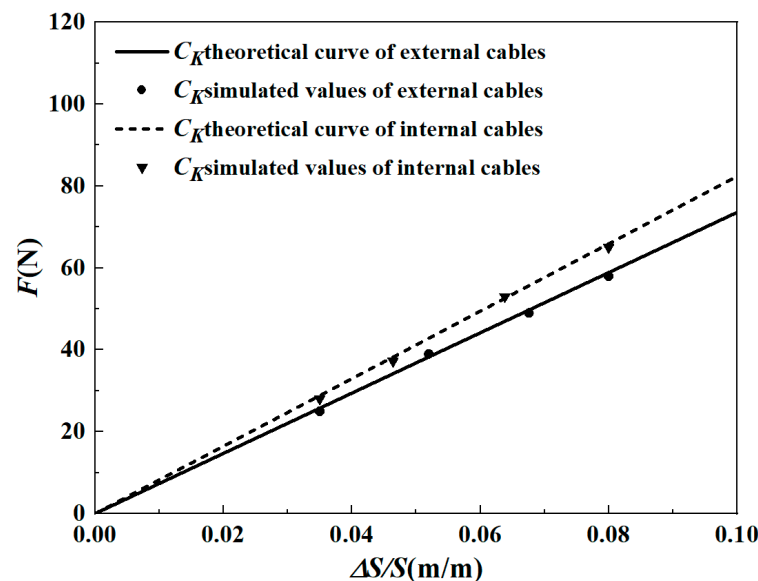
the vertical, as shown in Figure 1c. The system is in equilibrium when the initial tension of each cable is F_0 = 11 N.

Mooring pattern C_{M3}: There are four cables at either end of the horizontal cylinder, all the cables are diagonal, where the diagonal cables are at 45° to the vertical, as shown in Figure 1d. The system is in equilibrium when the initial tension of each cable is F_0 = 13 N.

The prototype mooring cable was a steel cable with a diameter of 174 mm, and the model mooring cable was simulated with a combination of wire rope, a fixed-length spring, and a unit counterweight. The fixed-length spring was configured to simulate the elongation of the mooring cable and the spring constant was determined from Equation (1) [19]. To simulate the model mooring cable, not only were the length and weight scaled, but the curve of mooring tension (T_m)–relative elongation (Δs) should also be matched. In order to accurately simulate the elasticity of mooring cables under the Froude similarity rule, the elastic characteristics of the prototype and model cables need to satisfy the following equation:

$$T_m = \frac{C_P d_P^2 (\Delta S/S)^n}{\lambda^3} \tag{1}$$

where T_m is the mooring tension of the model cable (N), C_P is the elasticity coefficient of the prototype cable (for steel cable, C_P = 26.97 × 10^4 MPa), d_P is the diameter of the prototype cable (m), $\Delta S/S$ is the relative elongation of the cable, and n is the index with the steel cable adopting n = 1.5. An example of a theoretical mooring tension–relative elongation curve and measured scatters for the case of C_{M3} are presented in Figure 2. It shows that excellent agreement was achieved. Figure 3 shows the layout of the model SFT moored in the test tank.
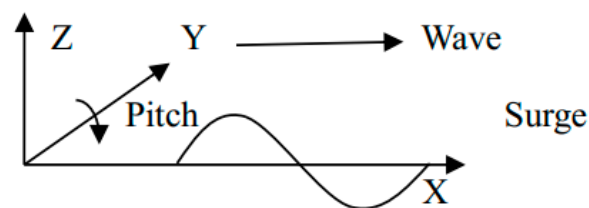

Figure 2. Theoretical and simulated mooring tension–relative elongation curve of the mooring cable for mooring pattern CM_3.

The experimental coordinate system is shown in Figure 4. The origin of the coordinate system is located at the center of the model. Positive x is along the wave propagation direction, positive z is vertical up along the water depth, and positive y is determined by the right-hand rule. For the two-dimensional test, three motion components were considered: surge, heave, and pitch. Surge is the longitudinal motion component along the x-axis (wave propagation direction is +x); heave is the vertical motion component along the z-axis (vertical up is +z); and pitch is the rotation around the y-axis (clockwise direction is +y).

Figure 3. The model SFT moored in test tank.

Figure 4. Experimental coordinate system.

2.3. Experimental Contents and Parameters

The experimental contents included the free decay tests aiming to determine the natural period of the mooring system, RAO tests (under regular wave), and dynamic response tests under irregular waves. Free decay tests were first conducted on the SFT with three degrees of freedom (surge, heave, and pitch) to obtain the natural periods and damping coefficients. The RAOs of the SFT were obtained through regular wave tests under the same test conditions as the free decay tests (in terms of water depth, submergence depth, mooring pattern, mooring stiffness, and initial tension of the mooring cable). For the tests, the water depth d and submergence depth d_0 were 120 cm and 42 cm, respectively. Correspondingly, the dimensionless submergence depth d_0/d was 0.35. The RAOs of the SFT were obtained through regular waves with an average wave height of $H = 4.0$ cm and an average period of $T = 0.8$ s~2.0 s. Three types of mooring patterns (C_{M1}, C_{M2}, and C_{M3}) were considered. The experimental parameters are summarized in Table 2. Based on the results of free decay tests and RAO tests, the dynamic responses under irregular waves

were tested to further compare the optimal mooring pattern and submergence depth. The experimental parameters are summarized in Tables 3 and 4. For submergence depth tests, the initial tension F_0 of each cable was 13 N. T_{0s}, T_{0H}, and T_{0p} are the natural periods of surge, heave, and pitch, respectively.

Table 2. Experimental parameters for the RAO tests (under regular waves).

Mooring Pattern CM_i	Initial Tension F_0 (N)	Average Period $\bar{T}$ (s)	Wavelength L (m)	Relative Submergence Depth d_0/L
CM_1	17	0.8	0.99	0.360
		1.0	1.56	0.231
		1.2	2.24	0.161
		1.4	3.02	0.119
		1.6	3.84	0.094
		1.8	4.67	0.077
		2.0	5.49	0.066
CM_2	11	0.8	0.99	0.360
		1.0	1.56	0.231
		1.2	2.24	0.161
		1.4	3.02	0.119
		1.6	3.84	0.094
		1.8	4.67	0.077
		2.0	5.49	0.066
CM_3	13	0.8	0.99	0.360
		1.0	1.56	0.231
		1.2	2.24	0.161
		1.4	3.02	0.119
		1.6	3.84	0.094
		1.8	4.67	0.077
		2.0	5.49	0.066

Table 3. Experimental parameters for mooring optimization (under irregular waves).

Mooring Pattern CM_i	Initial Tension F_0 (N)	Significant Wave Height H_S (cm)	Spectrum Peak Period T_P (s)	Relative Wave Height		Relative Period			Relative Submergence Depth d_0/L_P
				H_S/d	H_S/d_0	T_P/T_{0S}	T_P/T_{0H}	T_P/T_{0P}	
CM_1	17	4.0	0.8	0.033	0.095	0.39	0.40	0.39	0.420
			1.0			0.49	0.50	0.49	0.269
			1.2			0.58	0.60	0.59	0.188
			1.4			0.68	0.70	0.68	0.139
			1.6			0.78	0.80	0.78	0.109
			1.8			0.87	0.90	0.88	0.090
			2.0			0.98	1.00	0.98	0.077
		1.0	1.6	0.008	0.024	0.78	0.80	0.78	0.109
		2.0		0.017	0.048				
		3.0		0.025	0.071				
		4.0		0.033	0.095				
CM_2	11	4.0	0.8	0.033	0.095	0.49	0.52	0.45	0.420
			1.0			0.62	0.65	0.56	0.269
			1.2			0.74	0.77	0.67	0.188
			1.4			0.86	0.90	0.79	0.139
			1.6			0.99	1.03	0.90	0.109
			1.8			1.11	1.16	1.01	0.090
			2.0			1.23	1.29	1.12	0.077
		1.0	1.6	0.008	0.024	0.99	1.03	0.90	0.109
		2.0		0.017	0.048				
		3.0		0.025	0.071				
		4.0		0.033	0.095				
		5.0		0.042	0.120				
CM_3	13	4.0	0.8	0.033	0.095	0.67	0.67	1.60	0.420
			1.0			0.83	0.83	2.00	0.269
			1.2			1.00	1.00	2.40	0.188
			1.4			1.17	1.17	2.80	0.139
			1.6			1.33	1.33	3.20	0.109
			1.8			1.50	1.50	3.60	0.090
			2.0			1.67	1.67	4.00	0.077
		2.0	1.6	0.017	0.048	1.25	1.23	2.96	0.109
		3.0		0.025	0.071				
		4.0		0.033	0.095				
		5.0		0.042	0.119				
		6.0		0.050	0.143				
		7.0		0.058	0.167				
		8.0		0.067	0.190				

Table 4. Experimental parameters for relative submergence depth (under irregular waves).

Significant Wave Height H_S (cm)	Spectrum Peak Period T_P (s)	Relative Wave Height		Relative Period			Relative Submergence Depth d_0/L_P
		H_S/d	H_S/d_0	T_P/T_{0S}	T_P/T_{0H}	T_P/T_{0P}	
8.0	0.8	0.066	0.190	0.63	0.62	1.60	0.420
	1.0			0.78	0.77	2.00	0.269
	1.2			0.94	0.92	2.40	0.188
	1.4			1.09	1.08	2.80	0.139
	1.6			1.25	1.23	3.20	0.109
	1.8			1.41	1.38	3.60	0.090
	2.0			1.56	1.54	4.00	0.077
	2.2			1.72	1.69	4.40	0.067
	2.4			1.88	1.85	4.80	0.059
	2.6			2.03	2.00	5.20	0.054
2.0	1.6	0.017	0.048	1.25	1.23	3.20	0.109
3.0		0.025	0.071				
4.0		0.033	0.095				
5.0		0.042	0.119				
6.0		0.050	0.143				
7.0		0.058	0.167				
8.0		0.067	0.190				
9.0		0.075	0.214				
10.0		0.083	0.238				

3. Results and Discussion

3.1. Free Decay Test and RAO Test Results

With the three mooring patterns (CM_1, CM_2, CM_3) as shown in Figure 1, the natural periods, damping coefficients, and RAOs of the SFT could be obtained and analyzed based on the free decay tests and RAO tests of the SFT. It should be noted that the hydrostatic equilibrium of the SFT was upheld by counterbalancing the vertical components of the mooring tension against the net buoyancy force of the SFT.

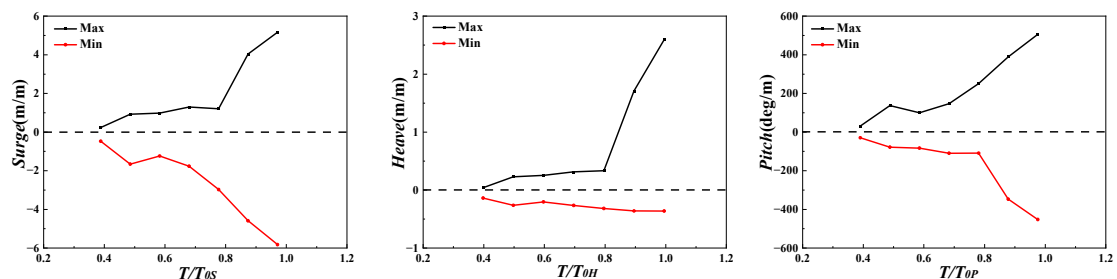#### 3.1.1. Natural Period and Damping Coefficient

The decay test was performed by applying an artificial displacement/rotation on the floater and releasing it in still water. The decay curve of the motion process had been completely collected until the moored SFT resumed to the static state. The natural periods and damping coefficients of surge, heave, and pitch were analyzed and are summarized in Table 5. Theoretically, the larger the stiffness of the mooring system, the smaller its natural period is. The natural periods of the three mooring systems were in the order of $CM_1 > CM_2 > CM_3$. The natural periods of surge and heave for mooring pattern CM_3 were approximately 50% of that for mooring pattern CM_1, and the natural period of pitch was only approximately 25% of that for mooring pattern CM_1. In addition, the natural period of the pitch was significantly shorter than those of the surge and heave, indicating that mooring system CM_3 had a strong constraint effect on the pitch. Table 5 shows that no considerable differences were observed in terms of the damping coefficients of surge and heave for three mooring patterns. However, considerable differences were observed in the damping coefficient of pitch. The damping coefficient of pitch for mooring pattern CM_3 was larger than those of mooring patterns CM_1 and CM_2, with a difference of approximately 30%.

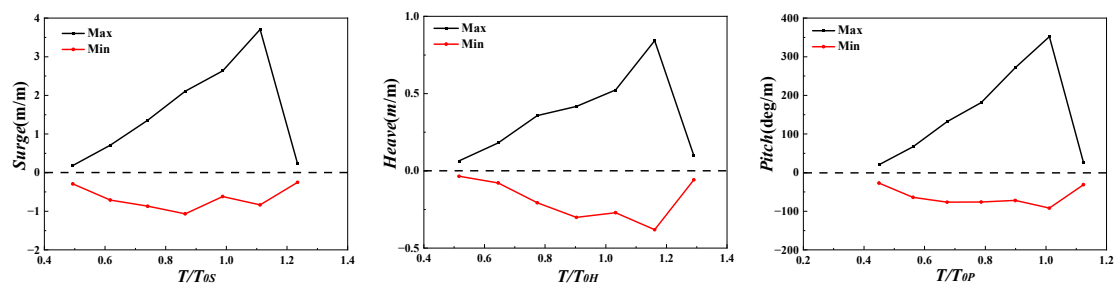**Table 5.** Natural period and damping coefficient of the SFT with different mooring patterns.

Mooring Pattern C_{Mi}	Surge		Heave		Pitch	
	Natural Period (s)	Damping Coefficient	Natural Period (s)	Damping Coefficient	Natural Period (s)	Damping Coefficient
C_{M1}	2.06	0.09	2.01	0.10	2.05	0.15
C_{M2}	1.62	0.08	1.55	0.11	1.78	0.16
C_{M3}	1.28	0.11	1.30	0.09	0.54	0.22

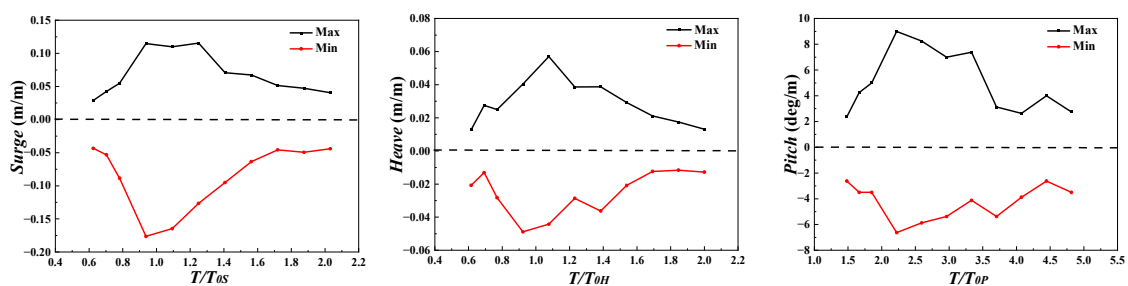3.1.2. Response Amplitude Operators (RAOs)

The RAOs of the SFT under different mooring patterns were obtained through regular wave tests. The water depth was fixed at $d = 1.2$ m and the submergence depth $d_0 = 42$ cm ($d_0/d = 0.35$, $d_0/D = 2.1$, where D is the diameter of the horizontal cylinder). The wave height in the test was selected as $H = 4.0$ cm, with average period $T = 0.8 \sim 2.0$ s. The period interval for each test was 0.2 s. Due to the limitation of the wave maker, the test period cannot cover the natural period of pitch under mooring pattern C_{M3}. Figure 5 shows the RAO test results of the SFT under three mooring patterns. The abscissas of the RAO curves for surge, heave, and pitch were dimensionless with their respective natural periods, and the abscissas of the RAO curves for mooring tension were dimensionless with the natural period of surge. The ordinate represents the dynamic response values under unit height waves. Max and Min RAO represent the maximum positive value and minimum negative value of the corresponding motion response in the RAO tests, respectively.

(**a**) RAOs of mooring pattern C_{M1}

(**b**) RAOs of mooring pattern C_{M2}

(**c**) RAOs of mooring pattern C_{M3}

(**d**) RAOs of upstream mooring tension   (**e**) RAOs of downstream mooring tension

Figure 5. RAOs of the SFT under three mooring patterns.

As shown in Figure 5, in terms of mooring patterns C_{M1} and C_{M2}, the maximum surge, heave, and pitch of the SFT occur at their natural periods and the RAO variations of the three motion components were similar. In terms of mooring pattern C_{M3}, the maximum surge and heave occurred at their natural periods and the RAO variations of the three motion components were similar. However, within the range of the wave period in the experiment, the maximum pitch occurred at $T_p/T_{0P} \approx 2.0$, twice the natural period of pitch. The maximum pitch occurred almost synchronously with the maximum surge and heave ($T_p/T_{0S} \approx 1.0$, $T_p/T_{0H} \approx 1.0$, $T_p/T_{0P} \approx 2.0$), indicating a significant coupling effect among the natural periods of the three motion components. Simultaneously, the RAO variations in the mooring tension were nearly identical to those of the surge, with the maximum mooring tension appearing near $T_p/T_{0S} \approx 1.0$. The RAOs of all tested dynamic response parameters under mooring pattern C_{M3} were significantly shorter than those under C_{M1} and C_{M2}. In other words, mooring pattern C_{M3} effectively restricted the motion response of the SFT, while the mooring tension was also less than those of C_{M1} and C_{M2}. This shows that mooring pattern C_{M3} was optimal in terms of RAOs.

3.2. Optimization Analysis of the Mooring Pattern

Section 3.1 describes the RAO tests and the results showed that of the mooring patterns, C_{M3} was the most optimal. Next, the advantages and disadvantages of the three mooring patterns were further comprehensively investigated through irregular wave tests in terms of three factors: the maximum value and spectral area of the motion response, the maximum value and uniformity of the mooring tension, and the length of time during which the cable reached a relaxed condition during wave action.

3.2.1. Motion Response of the SFT under Three Mooring Patterns

(1) The maximum motion response
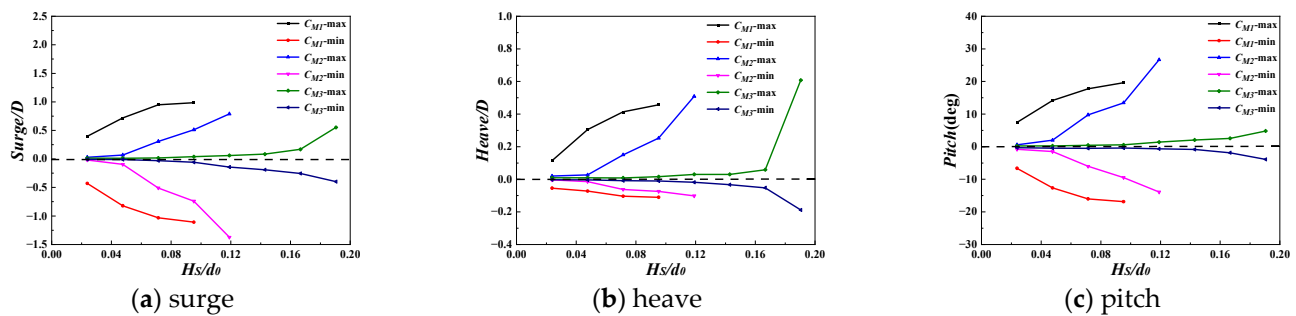
For the tests, the water depth was fixed at $d = 1.2$ m and the submergence depth $d_0 = 42$ cm ($d_0/d = 0.35$, $d_0/D = 2.1$). Two irregular wave series were generated, one wave series with the characteristics of $T_P = 1.6$ s and $Hs/d_0 = 0.02$~0.19, and the second wave series with the characteristics of $Hs = 4.0$ cm ($Hs/d_0 = 0.10$) and $T_P = 0.8$~2.0 s. The detailed wave parameters in the experiments are summarized in Table 6.

Table 6. The 0th-order moments (spectral areas) of the motion response varying with the relative wave height.
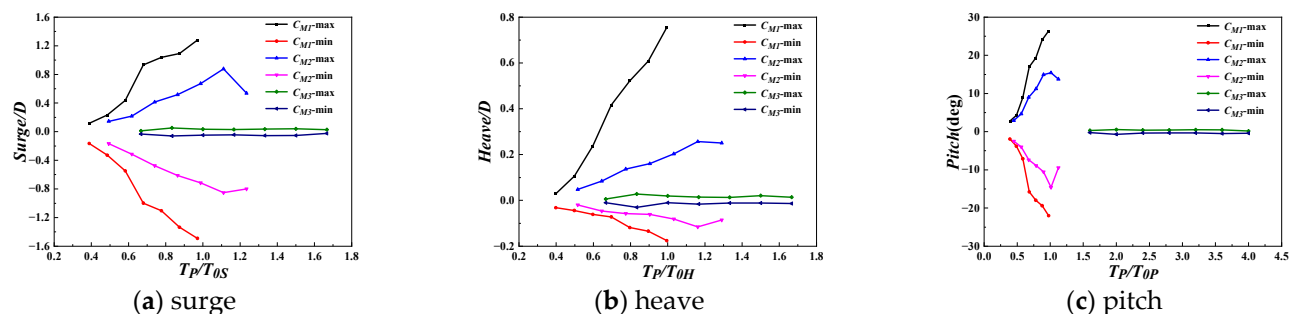
Significant Wave Height H_S (cm)	Relative Wave Height H_S/d	Spectrum Peak Period T_P (s)	Surge m_0 (cm²)			Heave m_0 (cm²)			Pitch m_0 (deg²)		
			C_{M1}	C_{M2}	C_{M3}	C_{M1}	C_{M2}	C_{M3}	C_{M1}	C_{M2}	C_{M3}
2.0	0.017		191.84	0.46	0.06	9.83	0.07	0.00	138.68	0.74	0.02
3.0	0.025	1.6 s	347.69	15.98	0.06	20.11	1.09	0.01	252.20	18.51	0.03
4.0	0.033		453.88	53.41	0.13	28.21	3.34	0.02	325.42	52.69	0.05

Figure 6 shows the statistical characteristic values of the surge, heave, and pitch of the SFT induced by the irregular wave versus the relative wave height under three mooring patterns. Figure 7 shows the statistical characteristic values of the surge, heave, and pitch of the SFT induced by the irregular wave versus the relative period under three mooring patterns. In Figure 6, the surge, heave, and pitch of the SFT are all significantly correlated with the relative wave height. The positive and negative maximum values of each motion component increase nonlinearly as the relative wave height increases under three mooring patterns. Moreover, the maximum motion responses under three mooring patterns remain in the order of $C_{M1} > C_{M2} > C_{M3}$. In addition, Figure 6 shows that mooring pattern C_{M3} constrains the heave of the 2D SFT relatively well, even though all the cables of the mooring system are diagonal, where the diagonal cables are at 45° to the vertical, as shown in Figure 1d. Mooring pattern C_{M3} not only has an overwhelming advantage over the other two mooring patterns in limiting the surge and pitch of the 2D SFT, but it also has a better constraint on heave than the C_{M1} and C_{M2} mooring patterns. It should be noted that

regardless of the presence or absence of vertical cables, all the three mooring patterns show a tendency in which the heave of the 2D SFT increases significantly with an increase in H_S/d_0 after a certain relative wave height is reached.

Figure 6. The motion responses of the SFT versus the relative wave height (d = 1.2 m, d_0 = 42 cm, d_0/d = 0.35, T_P = 1.6 s).

Figure 7. The motion responses of the SFT versus the relative period (d = 1.2 m, d_0 = 42 cm, d_0/d = 0.35, H_s/d_0 = 0.10).

In Figure 7, a comparison of the statistical characteristic values of the motion response versus the relative period under three mooring patterns revealed that C_{M3}, for which the range of test periods was approximately 1.5~4.0 times the natural period of the motion components, had an overwhelming advantage over the other two mooring patterns in terms of restraining the motion response.

(2) Spectral area of the motion response

The statistical characteristic values of the motion response of the 2D SFT versus relative wave height and relative period under three mooring patterns were previously discussed. In this section, based on the measured time histories, spectral analyses were performed to obtain the frequency-domain characteristics of the motions of the SFT. The spectral areas for the three types of mooring patterns were compared for the global analysis of motion responses.

Tables 6 and 7 list the 0th-order moments (spectral areas) of each motion response component of the 2D SFT under three mooring patterns varying with the relative wave height (spectral peak period is fixed) and relative periods (significant wave height is fixed), respectively.

From Tables 6 and 7, it can be seen that the 0th-order moments (spectral areas) of the motion response are in the order of $C_{M1} > C_{M2} > C_{M3}$ from largest to smallest. For mooring pattern C_{M3}, the 0th-order moments (spectral areas) for all three motion components were significantly smaller than those of the other two mooring patterns and the difference was particularly significant for large wave actions.
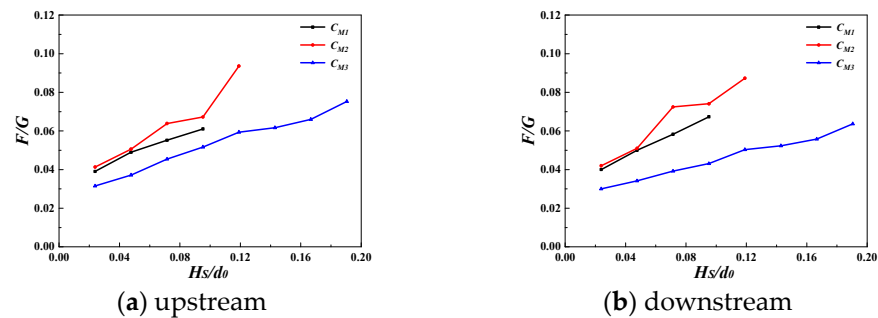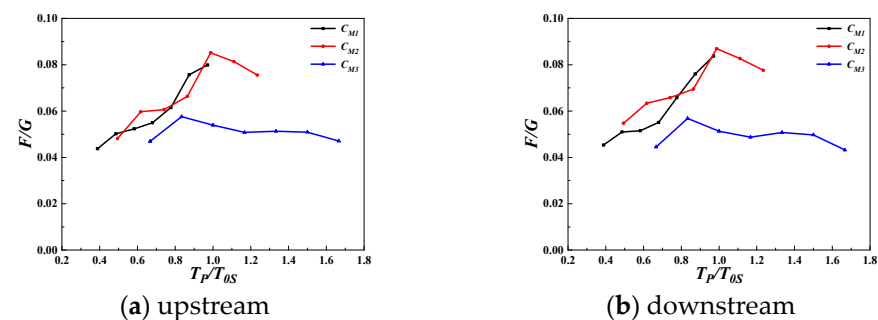
Combining the test results in Figures 6 and 7 and Tables 6 and 7, it can be concluded that C_{M3} was the optimal pattern of the three mooring patterns in terms of restraining the motion response of the 2D SFT.

Table 7. The 0th-order moments (spectral areas) of the motion response varying with the relative period.

Significant Wave Height H_S (cm)	Relative Wave Height H_S/d	Spectrum Peak Period T_P (s)	Surge m_0 (cm²)			Heave m_0 (cm²)			Pitch m_0 (deg²)		
			C_{M1}	C_{M2}	C_{M3}	C_{M1}	C_{M2}	C_{M3}	C_{M1}	C_{M2}	C_{M3}
4.0	0.033	0.8	4.49	5.30	0.04	0.21	0.21	0.01	3.01	4.13	0.01
		1.0	13.83	12.71	0.13	0.65	0.53	0.04	9.25	12.61	0.07
		1.2	55.54	31.02	0.14	2.64	1.28	0.03	37.77	30.96	0.06
		1.4	231.05	48.01	0.14	12.86	1.79	0.02	161.73	46.12	0.05
		1.6	478.50	56.70	0.13	29.72	2.93	0.02	341.80	56.09	0.05
		1.8	672.05	57.10	0.12	44.77	3.01	0.01	493.60	57.24	0.03
		2.0	801.98	28.25	0.09	60.93	1.82	0.01	626.99	30.75	0.03

3.2.2. Mooring Tension and Its Uniformity of Distribution under Three Mooring Patterns

In this section, the mooring tension of the upstream (1#) and downstream (3# and 4#) cables of the SFT were selected as representatives for discussion. The mooring tensions of the other cables were described in the uniformity of the mooring tension. The test conditions were the same as those described in Section 3.2.1. Figure 8 shows the statistical characteristic values of the upstream (#1) and downstream (#4) mooring tension of the SFT induced by the irregular wave versus the relative wave height under three mooring patterns. Figure 9 shows the statistical characteristic values of the upstream (#1) and downstream (#4) mooring tension of the SFT induced by the irregular wave versus the relative period under three mooring patterns.

(**a**) upstream (**b**) downstream

Figure 8. The statistical characteristic values of the upstream (1#) and downstream (3# and 4#) mooring tensions versus the relative wave height (d = 1.2 m, d_0 = 42 cm, d_0/d = 0.35, T_P = 1.6 s).

(**a**) upstream (**b**) downstream

Figure 9. The statistical characteristic values of the upstream (#1) and downstream (3# and 4#) mooring tensions versus the relative period (d = 1.2 m, d_0 = 42 cm, d_0/d = 0.35, H_S/d_0 = 0.10).

Figures 8 and 9 show that the maximum mooring tension of mooring patterns C_{M1} and C_{M2} were generally the same and the maximum mooring tension transferred from each other alternatively with relative wave height and relative period. However, both mooring patterns yielded a larger mooring tension as compared with mooring pattern C_{M3}. Tables 8 and 9 list the 0th-order moments (spectral areas) of upstream (1#) mooring tension of the SFT under three mooring patterns varying with the relative wave height (spectral peak period is fixed) and relative periods (significant wave height is fixed), respectively.

Tables 8 and 9 show that the 0th-order moments (spectral areas) of upstream (1#) mooring tension of mooring pattern C_{M3} were significantly smaller than those of the other two mooring patterns.
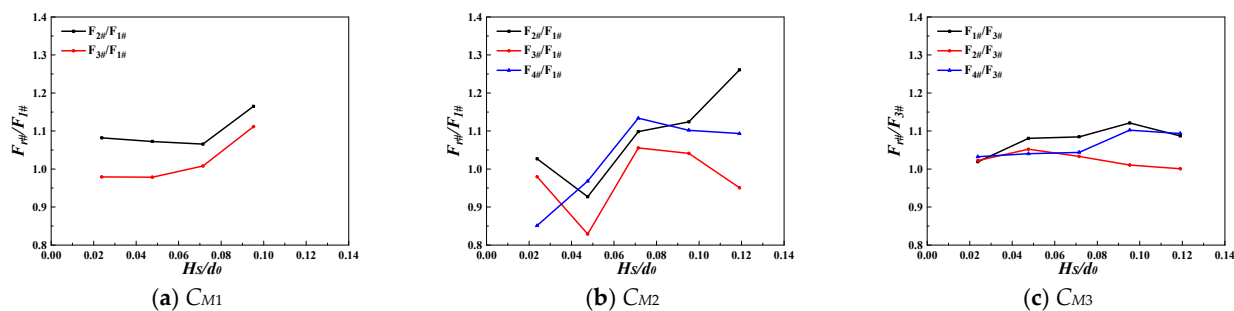
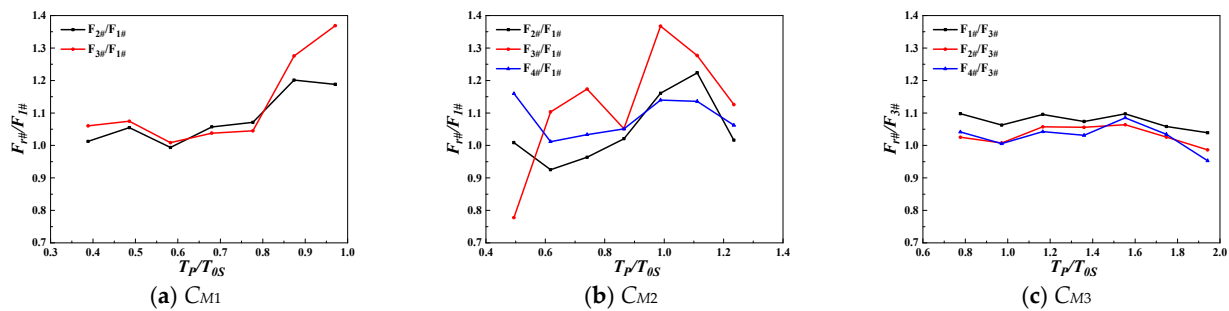**Table 8.** The 0th-order moments (spectral areas) of upstream (#1) mooring tension varying with the relative wave height.

Significant Wave Height H_S (cm)	Relative Wave Height H_S/d	Spectrum Peak Period T_P (s)	Mooring Tension m_0 (N^2)		
			C_{M1}	C_{M2}	C_{M3}
2.0	0.017		56.70	68.03	13.00
3.0	0.025	1.6	107.45	192.88	29.71
4.0	0.033		156.73	295.10	54.25

Table 9. The 0th-order moments (spectral areas) of upstream (#1) mooring tension varying with the relative periods.

Significant Wave Height H_S (cm)	Relative Wave Height H_S/d	Spectrum Peak Period T_P (s)	Mooring Tension m_0 (N^2)		
			C_{M1}	C_{M2}	C_{M3}
		0.8	8.97	7.22	8.29
		1.0	17.13	136.02	50.65
		1.2	28.30	229.30	56.72
4.0	0.033	1.4	75.54	269.19	56.73
		1.6	161.53	312.87	53.97
		1.8	255.70	314.55	47.12
		2.0	407.27	269.14	41.49

The uniformity of the mooring tension is a major factor in determining the optimal mooring pattern. For the two-dimensional case, the cables at either end of the horizontal cylinder were basically the same. Therefore, the mooring tension of all cables at one end was selected for discussion. The dimensionless mooring tensions were used to account for the uniformity of the mooring tension, expressed as $F_{r\#}/F_{i\#}$, where *i#* denotes the cable with the minimum mooring tension for most cases at one end, and *r#* denotes the other cables. Figures 10 and 11 show the dimensionless mooring tensions versus the relative wave heights and relative periods under three mooring patterns, respectively.

| (a) C_{M1} | (b) C_{M2} | (c) C_{M3} |

Figure 10. The dimensionless mooring tensions versus the relative wave heights ($d = 1.2$ m, $d_0 = 42$ cm, $d_0/d = 0.35$, $T_P = 1.6$ s).
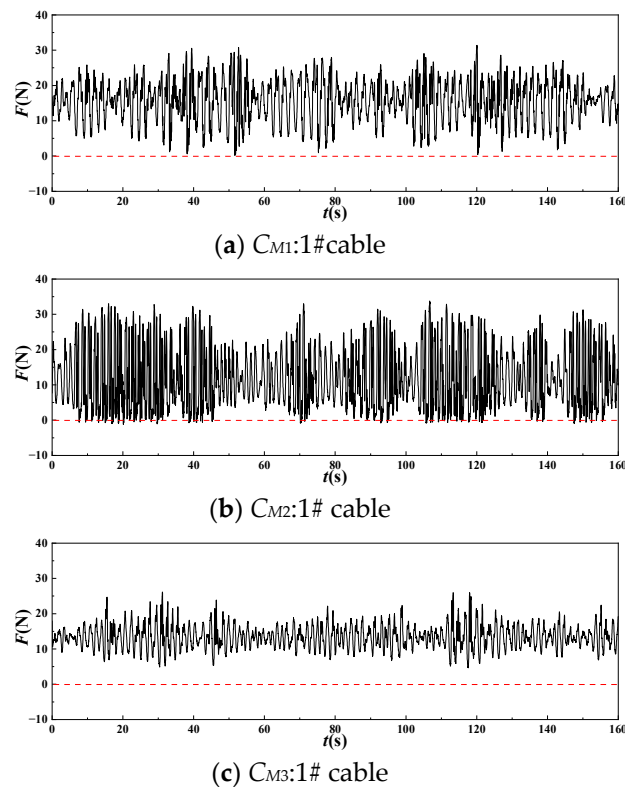
From Figures 10 and 11, the dimensionless mooring tensions ($F_{r\#}/F_{i\#}$) of all the cables under three mooring patterns were C_{M1}: 1.0~1.36, C_{M2}: 0.8~1.37, and C_{M3}: 1.0~1.12. The results reveal that the uniformity of the mooring tension for mooring pattern C_{M3} was better than those for the other two mooring patterns.
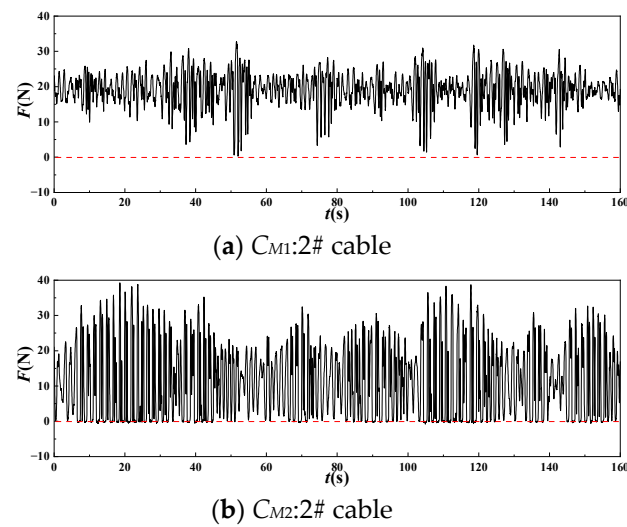
(**a**) C_{M1} (**b**) C_{M2} (**c**) C_{M3}

Figure 11. The dimensionless mooring tensions versus the relative periods (d = 1.2 m, d_0 = 42 cm, d_0/d = 0.35, H_S/d_0 = 0.10).

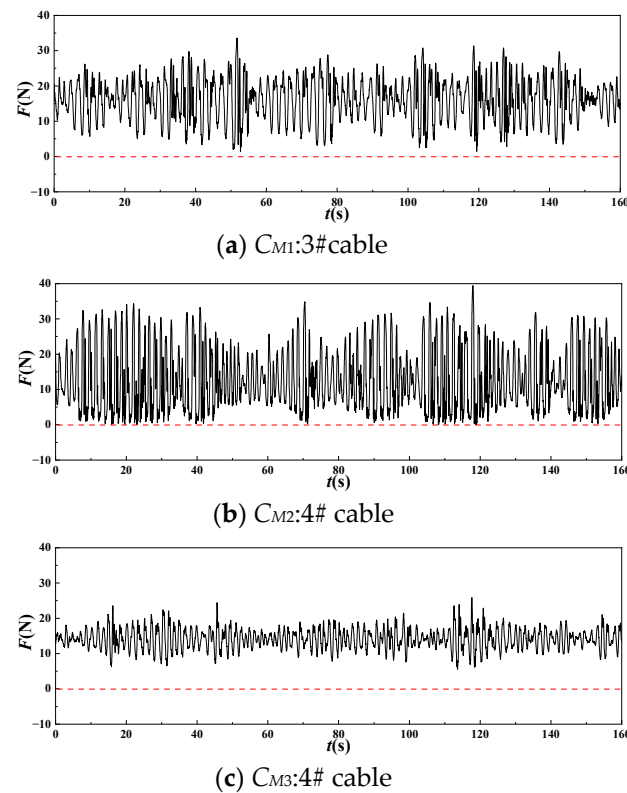### 3.2.3. The Relaxed Time of the Cables under the Three Mooring Patterns

Figures 12–14 show the time history of the upstream (1#) mooring tension under C_{M1}, C_{M2}, and C_{M3}; the vertical (2#) mooring tension under C_{M1} and C_{M2}; and the downstream (C_{M1}: 3#, C_{M2} and C_{M3}: 4#) mooring tension under C_{M1}, C_{M2}, and C_{M3}. From Figures 12–14, the cables under mooring pattern C_{M2} exhibited the longest relaxed time, while the relaxed time for mooring pattern C_{M3} was shortest. The relaxed time for mooring pattern C_{M1} was centered among three types of mooring patterns. The relaxed time means the length of time during which the cable reached a relaxed condition during wave action. It should be noted that when the 2D SFT moved vertically downward, the cable reached a relaxed state; therefore, compared with mooring pattern C_{M1}, an additional vertical cable was not more effective in constraining the vertically downward movement of the 2D SFT. Furthermore, the vertical combined initial tension was equal to the net buoyancy of the 2D SFT, and the initial tension of the cables under C_{M2} (F_0 = 11 N) was less than that of the cables under C_{M1} (F_0 = 17 N), which makes the cables more susceptible to a relaxed state.

(**a**) C_{M1}:1#cable

(**b**) C_{M2}:1# cable

(**c**) C_{M3}:1# cable

Figure 12. The time history of the upstream (#1) mooring tension under C_{M1}, C_{M2}, and C_{M3} (Hs = 4.0 cm, T_P = 1.6 s, d = 1.2 m, d_0 = 42 cm, d_0/d = 0.35).

(a) C_{M1}:2# cable

(b) C_{M2}:2# cable

Figure 13. The time history of the vertical (2#) mooring tension under C_{M1} and C_{M2} (Hs = 4.0 cm, T_P = 1.6 s, d = 1.2 m, d_0 = 42 cm, d_0/d = 0.35).

(a) C_{M1}:3#cable

(b) C_{M2}:4# cable

(c) C_{M3}:4# cable

Figure 14. The time history of the downstream mooring tension under C_{M1}, C_{M2}, and C_{M3} (C_{M1}: 3#, C_{M2} and C_{M3}: 4#; Hs = 4.0 cm, T_P = 1.6 s, d = 1.2 m, d_0 = 2 cm, d_0/d = 0.35).

In summary, according to the comparison of three types of mooring patterns in terms of the maximum value and spectral area of the motion response, the maximum value and uniformity of the mooring tension, and the relaxed time of the cables, mooring pattern C_{M3} was determined to be the optimal mooring pattern.

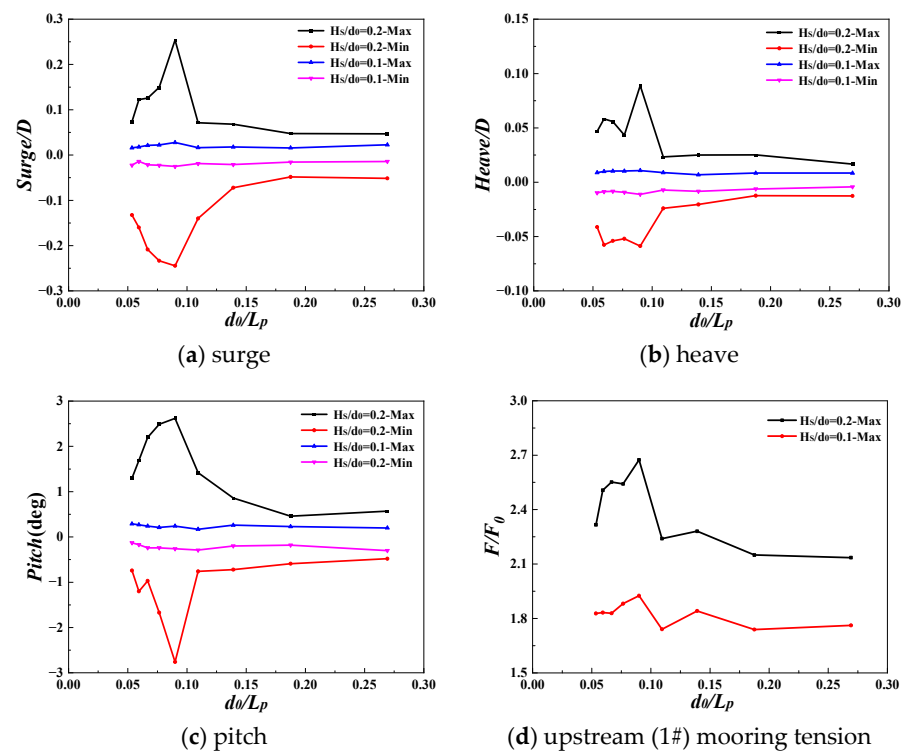### 3.3. Optimization Analysis of the Submergence Depth

As mooring pattern C_{M3} was determined to be the best of the three mooring patterns, in this section, the correlation between the dynamic responses of the SFT and the dimensionless parameters (the dimensionless submergence depth, period and wave height, KC

number) for mooring pattern C_{M3} is further investigated and an effective method is subsequently devised for determining the optimal submergence depth in the engineering context.

3.3.1. Variation in the Dynamic Response with Relative Submergence Depth d_0/L_P

For the tests, the water depth was fixed at $d = 1.2$ m and the submergence depth $d_0 = 42$ cm ($d_0/d = 0.35$, $d_0/D = 2.1$). The irregular wave series were generated with the characteristics of the spectrum peak periods $T_P = 1.0{\sim}2.6$ s (the relative periods $T_P/T_{0S} = 0.63{\sim}2.03$, $T_P/T_{0H} = 0.62{\sim}2.00$, $T_P/T_{0P} = 1.60{\sim}5.20$; the relative submergence depth $d_0/L_P = 0.05{\sim}0.27$) and the significant wave heights $Hs = 4.0$ cm and 8.0 cm (the relative wave height $Hs/d_0 = 0.10$ and 0.2). The detailed wave parameters in the experiments are summarized in Table 4.

Figure 15 shows the statistical characteristic values of the surge, heave, pitch, and upstream (1#) mooring tension of the SFT induced by the irregular wave versus the relative submergence depth d_0/L_P. According to the analytical solution, increasing draft can sufficiently restrain the motion response and tether stress of the SFT [20]. Consistently, the present experimental results suggest that when the relative wave height is smaller ($Hs/d_0 = 0.10$), the motion response of the SFT remains basically unchanged and maintains a stable and small value within the range of the relative submergence depths in the experiment, where the surge is less than 0.015D (D denotes the diameter of the horizontal cylinder), the heave is less than 0.01D, and the pitch is less than 0.3°. The mooring tension of the cable oscillates slightly in the range of $d_0/L_P \leq 0.15$, with the oscillation amplitude ranging from 1.7 to $2.0F_0$ (F_0 denotes the initial tension $F_0 = 13$ N), and then gradually decreases to a smaller value ($1.7F_0$) as the relative submergence depth increases.

Figure 15. The dynamic response versus the relative submergence depth d_0/L_P ($T_P = 1.0{\sim}2.6$ s, $d_0 = 42$ cm, $d_0/d = 0.35$).
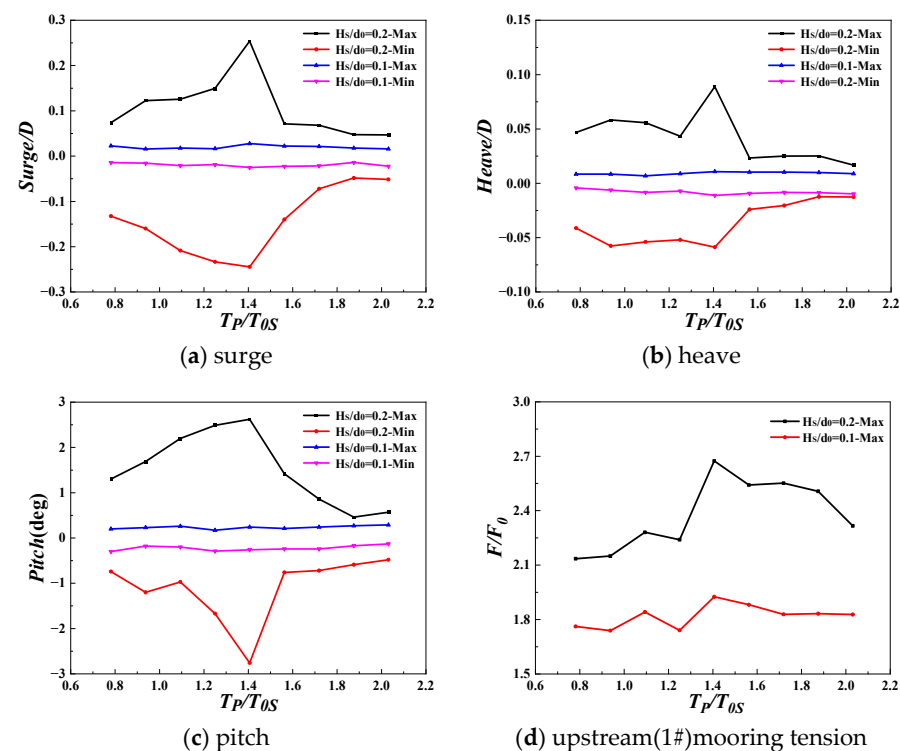
As the relative wave height increases to $Hs/d_0 = 0.20$, the dynamic response characteristic can be distinguished into two parts bounded by $d_0/L_P \approx 0.15$ within the range of the relative submergence depth in the experiment. Within the interval of $d_0/L_P \leq 0.15$, all the dynamic response components oscillated considerably, with relatively high peak values occurring in the interval of $d_0/L_P = 0.07{\sim}0.10$ (where the surge is 0.25D, heave is

0.10D, pitch is 2.8°, and mooring tension is 2.7F_0). Within the interval of $d_0/L_P > 0.15$, the dynamic response gradually decreases to a relatively stable value with an increase in relative submergence depth (where the surge is basically stable at 0.07D, heave is basically stable at 0.03D, pitch is basically stable at 0.9°, and mooring tension is basically stable at 2.0F_0). The present experimental results suggest that there exists an "appropriate" relative submergence depth where the dynamic responses of the SFT are minimal for a certain Hs/d_0. Notably, under this submergence depth, the dynamic responses remain unaffected by the variation in the wave period. In the experiment, when $Hs/d_0 = 0.2$, the "appropriate" relative submergence depth is $d_0/L_P \geq 0.15$.

3.3.2. Variation in the Dynamic Response with Relative Period

The relative submergence depth can be defined by the ratio of the absolute submergence depth to the wavelength, represented as d_0/L_P. The wavelength is influenced by the water depth and wave period. This implies that the impact of relative submergence depth on dynamic response is essentially the wave period.

In this section, the ratio of spectrum peak period T_P and the natural period of surge T_{0S} (which is also the natural period of the heave T_{0H}) is taken as the abscissa, and the dynamic response of the SFT induced by the irregular wave versus the relative period under the experimental conditions consistent with Section 3.3.1 are graphed in Figure 16.

Figure 16. The dynamic response versus the relative wave period ($T_P = 1.0 \sim 2.6$ s, $d_0 = 42$ cm, $d_0/d = 0.35$).

As shown in Figure 16, when the relative wave height is smaller ($Hs/d_0 = 0.10$), the motion response of the SFT remains basically unchanged and maintains a stable and small value within the range of the relative period in the experiment, where the surge is less than 0.015D, the heave is less than 0.01D, and the pitch is less than 0.3°. The mooring tension of the cable oscillates slightly in the range of the relative period in the experiment, with the oscillation amplitude ranging from 1.7 to 2.0F_0 (F_0 denotes the initial tension $F_0 = 13$ N).

With the relative wave height increasing to $Hs/d_0 = 0.20$, both the motion response and mooring tension exhibit a notable peak at $T_P/T_{0S} \approx 1.4$. The dynamic response exhibits significant fluctuations within the relative period range in the experiment. Notably, the
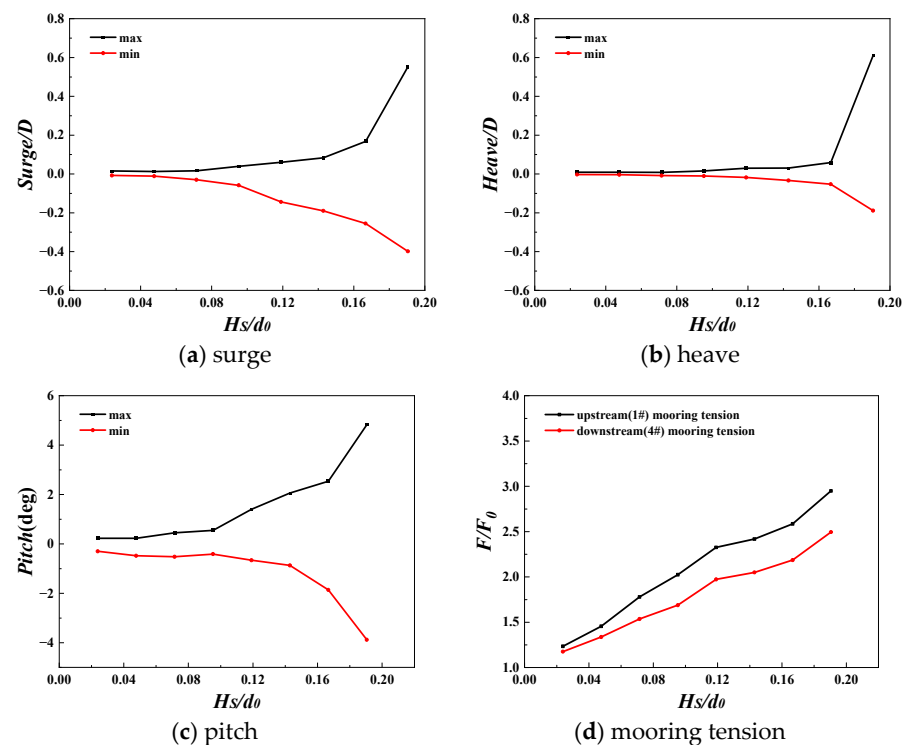
maximum motion response and mooring tension did not appear at the natural frequency of the surge, heave, and pitch (T_P/T_{0S} = 1.41, T_P/T_{0H} = 1.38, T_P/T_{0P} = 3.60). This discrepancy could be due to the combined influences of the system's natural frequency and the vortex release frequency.

3.3.3. Variation in the Dynamic Response with Relative Wave Height H_S/d_0

The relationship between wave height and absolute submergence depth, represented as H_S/d_0, is also an important influencing factor for the dynamic response of the SFT. In this section, the statistical characteristic of the dynamic response of the SFT varying with the relative wave height H_S/d_0 under irregular waves was investigated.

For the tests, the water depth was fixed at d = 1.2 m and the submergence depth was d_0 = 42 cm (d_0/d = 0.35, d_0/D = 2.1). The irregular wave series were generated with the characteristics of T_P = 1.6 s and Hs/d_0 = 0.02~0.19. Figure 17 shows the statistical characteristic of the surge, heave, pitch, and mooring tension of the SFT varying with the relative wave height H_S/d_0 under irregular waves. In Figure 17, the surge, heave, and pitch of the SFT are all significantly correlated with relative wave height H_S/d_0. The positive and negative maximum values of each motion component increase nonlinearly as the relative wave height increases. As shown in Figure 17, when the relative wave height H_S/d_0 is smaller ($Hs/d_0 \leq 0.10$), the motion response of the SFT remains basically unchanged and maintains a stable and small value within the range of relative wave height H_S/d_0, where the surge is less than 0.06D (D denotes the diameter of the horizontal cylinder), the heave is less than 0.02D, and the pitch is less than 0.6°. With the relative wave height Hs/d_0 > 0.10, the motion response increases nonlinearly as the relative wave height increases, which indicates that the relative wave height H_S/d_0 has significant effects on the motion responses. In addition, Figure 17 shows that the mooring system constrains the heave of the SFT well, even though all the cables are diagonal, where the diagonal cables are at 45° to the vertical, as shown in Figure 1d. Moreover, both the upstream and downstream mooring tensions of the SFT increase almost linearly with the increase in relative wave height H_S/d_0. Meanwhile, the upstream mooring tension is slightly larger than that of the downstream.

Figure 17. The dynamic response versus the relative wave height H_S/d_0 (T_P = 1.6 s, Hs/d_0 = 0.02~0.19, d_0 = 42 cm, d_0/d = 0.35).

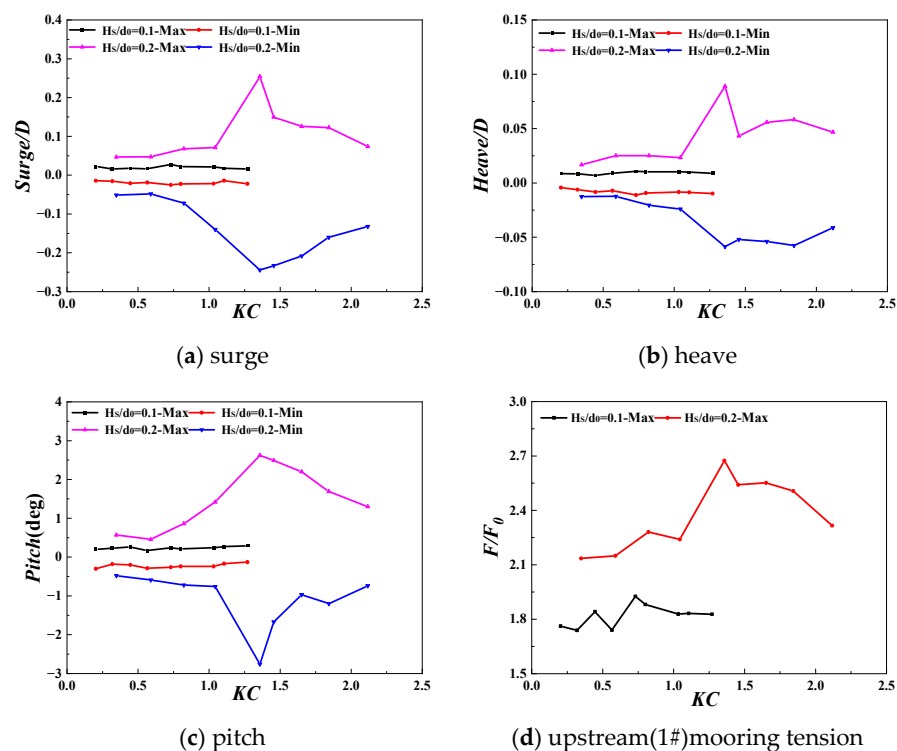### 3.3.4. Variation in the Dynamic Response with KC Number

Considering that the *KC* number can account for the wave height, wave period, and absolute submergence depth, it is introduced into this study to investigate the relationship between the dynamic response of the 2D SFT and *KC* number. The *KC* number is a key parameter for analyzing the hydrodynamic problems of the cylinder [21]. The *KC* number is defined as [22]

$$KC = \frac{u_{max}T}{D} \tag{2}$$

$$u(t) = \frac{\pi H}{T}\frac{coshkz}{sinhkd}\cos(kx - wt) \tag{3}$$

where u_{max} indicates the maximum horizontal velocity at the water level calculated by linear wave theory. H, T, k, and d denote the wave height, wave period, wave number, and water depth, respectively. z is the vertical coordinate with the bottom of the water $z = 0$ and the still water surface $z = d$. In the present study, the relevant parameters are specified as follows: the wave height is considered as the maximum wave height in the wave sequence; the period is considered as the spectrum peak period; and the location z is considered as the center of the SFT ($z = d - d_0 - D/2$, where d_0 represents the absolute submergence depth, d represents the water depth, and D represents the diameter of the horizontal cylinder).

Figure 18 shows the statistical characteristic of the surge, heave, pitch, and upstream (1#) mooring tension of the SFT induced by the irregular wave versus the *KC* number.

(a) surge   (b) heave

(c) pitch   (d) upstream(1#)mooring tension

Figure 18. The dynamic response versus the *KC* number (T_P = 1.0~2.6 s, d_0 = 42 cm, d_0/d = 0.35).

As shown in Figure 18, the variation in the surge, heave, pitch, and upstream (1#) mooring tension of the SFT with *KC* number is basically opposite to the variation in the dynamic response with relative submergence depth d_0/L_P. This is due to the fact that as the relative submergence depth d_0/L_P increases, the *KC* number decreases. Hence, opposite variations occur in the curves of the dynamic response with d_0/L_P and *KC* number as the abscissas.

Thus, a similar conclusion can be drawn: for a certain Hs/d_0, there exists an "appropriate" *KC* number, with which the dynamic response of the SFT varies significantly. In the experiment, the "appropriate" *KC* number is $KC \leq 0.8$ for $Hs/d_0 = 0.2$.

4. Conclusions

The present study focused on the anchor-cable SFT, and a series of experiments were conducted under regular and irregular waves. Based on the motion response and mooring tension derived from the tests, the effects of mooring pattern and submergence depth were examined comprehensively. Subsequently, the optimal mooring pattern and the submergence depth for the SFT were then determined. The main conclusions are summarized as follows:

(1) For the mooring system along the SFT, the pattern of diagonal cables is better than that of the diagonal cables + vertical cables. The 0th-order moments of the dynamic response are in the order of $C_{M1} > C_{M2} > C_{M3}$ from largest to smallest. The uniformity of the mooring tension of all the cables under mooring pattern C_{M3} is better than those of the other two mooring patterns. The length of the relaxed time for mooring pattern C_{M2} is longest, while that for mooring pattern C_{M3} is shortest.

(2) For the SFT subjected to waves, there is an "appropriate" relative submergence depth under which the dynamic responses remain relatively stable and are unaffected by the variation in the wave period. When the relative wave height is smaller ($Hs/d_0 = 0.10$), the motion response of the SFT remains basically unchanged and maintains a stable and small value within the range of relative submergence depths. With the relative wave height $Hs/d_0 = 0.20$, the "appropriate" submergence depth is $d_0/L_P > 0.15$. In the range of $d_0/L_P > 0.15$, the dynamic response gradually decreases to a relatively stable value with an increase in relative submergence depth. Under the same condition, if the KC number is used to determine the "appropriate" submergence depth, the KC number corresponds to $KC \leq 0.8$.

(3) With the relative wave height $Hs/d_0 = 0.20$, both the motion response and mooring tension exhibit a notable peak at $T_P/T_{0S} \approx 1.4$. The dynamic response exhibits significant fluctuations within the relative period range. Notably, the maximum motion response and mooring tension do not appear at the natural frequency of the surge, heave, and pitch ($T_P/T_{0S} = 1.41$, $T_P/T_{0H} = 1.38$, $T_P/T_{0P} = 3.60$). This discrepancy could be due to the combined influences of the system's natural frequency and the vortex release frequency.

Author Contributions: Conceptualization, C.C. (Cheng Cui); Methodology, C.C. (Cheng Cui); Validation, W.P.; Formal analysis, C.C. (Chun Chen); Investigation, W.P., C.C. (Cheng Cui), C.C. (Chun Chen), M.X. and Z.Y.; Data curation, Q.G.; Writing—original draft, W.P.; Writing—review & editing, C.C. (Cheng Cui). All authors have read and agreed to the published version of the manuscript.

Data Availability Statement: The data presented in this study are available on request from the corresponding author upon reasonable request.

Conflicts of Interest: The authors declare no conflicts of interest.

References

1. Sun, S.N. *Dynamic Response Analysis of Submerged Floating Tunnel*; Dalian University of Technology: Dalian, China, 2008.
2. Cao, C.F. *Dynamic Response Analysis and Experiment of Submerged Floating Tunnel Based on Fluid-Structure Interaction*; Zhejiang University: Hangzhou, China, 2013.
3. Wang, G.D. Numerical Analysis and Experiment Research of Submerged Floating Tunnel Subjected to Wave and Current Effect; Southwest Jiaotong University, Chengdu, China, 2008.
4. Russo, S.; Contestabile, P.; Bardazzi, A.; Leone, E.; Iglesias, G.; Tomasicchio, G.R.; Vicinanza, D. Dynamic Loads and Response of a Spar Buoy Wind Turbine with Pitch-Controlled Rotating Blades: An Experimental Study. *Energies* **2021**, *14*, 3598. [CrossRef]
5. Seo, S.I.; Mun, H.S.; Lee, J.H.; Kim, J.H. Simplified analysis for estimation of the behavior of a submerged floating tunnel in waves and experimental verification. *Mar. Struct.* **2015**, *44*, 142–158. [CrossRef]
6. Cifuentes, C.; Kim, S.; Kim, M.H.; Park, W.S. Numerical simulation of the coupled dynamic response of a submerged floating tunnel with mooring lines in regular waves. *Ocean Syst. Eng.* **2015**, *5*, 109–123. [CrossRef]

7.   Jeong, K.; Min, S.; Jang, M.; Won, D.; Kim, S. Feasibility study of submerged floating tunnels with vertical and inclined combined tethers. *Ocean Eng.* **2022**, *265*, 441–459. [CrossRef]

8.   Lee, J.; Jin, C.; Kim, M. Dynamic response analysis of submerged floating tunnels by wave and seismic excitations. *Ocean Syst. Eng.* **2017**, *7*, 1–19. [CrossRef]

9.   Muhammad, N.; Ullah, Z.; Choi, D.H. Performance Evaluation of Submerged Floating Tunnel Subjected to Hydrodynamic and Seismic Excitations. *Appl. Sci.* **2017**, *7*, 1122. [CrossRef]

10.   Jin, C.; Kim, M.H. Dynamic and structural responses of a submerged floating tunnel under extreme wave conditions. *Ocean Syst. Eng.* **2017**, *7*, 413–433.

11.   Won, D.; Seo, J.; Kim, S. Dynamic response of submerged floating tunnels with dual sections under irregular waves. *Ocean Eng.* **2021**, *241*, 110025. [CrossRef]

12.   Wu, Z.W.; Cheng, Z.Y.; Garg, A.; Jiang, M.J.; Meng, X.Z.; Mei, G.X. Investigating anti-vibration performance of a novel three-tube submerged floating tunnel reinforced with FRP rigid truss. *Ocean Eng.* **2023**, *269*, 113447. [CrossRef]

13.   Won, D.; Kim, S. Feasibility Study of Submerged Floating Tunnels Moored by an Inclined Tendon System. *Int. J. Steel Struct.* **2018**, *18*, 1191–1199. [CrossRef]

14.   Chen, Z.Y.; Xiang, Y.Q.; Lin, H.; Yang, Y. Coupled Vibration Analysis of Submerged Floating Tunnel System in Wave and Current. *Appl. Sci.* **2018**, *8*, 1311. [CrossRef]

15.   Deng, S.; Ren, H.J.; Xu, Y.W.; Fu, S.X.; Moan, T.; Gao, Z. Experimental study on the drag forces on a twin-tube submerged floating tunnel segment model in current. *Appl. Ocean. Res.* **2020**, *104*, 102326. [CrossRef]

16.   Yang, Z.W.; Li, J.Z.; Zhang, H.Q.; Yuan, C.G.; Yang, H. Experimental Study on 2D Motion Characteristics of Submerged Floating Tunnel in Waves. *J. Mar. Sci. Eng.* **2020**, *8*, 123. [CrossRef]

17.   Chen, X.B.; Chen, Q.; Chen, Z.W.; Cai, S.Q.; Zhuo, X.R.; Lv, J.E. Numerical modeling of the interaction between submerged floating tunnel and surface waves. *Ocean Eng.* **2021**, *220*, 108494. [CrossRef]

18.   Won, D.; Park, W.S.; Kang, Y.J.; Kim, S. Dynamic behavior of the submerged floating tunnel moored by inclined tethers attached to fixed towers. *Ocean Eng.* **2021**, *237*, 109663. [CrossRef]

19.   *JTS/T231-2021*; Technical Code of Modelling Test for Port and Waterway Engineering. China Communications Press: Beijing, China, 2021.

20.   Jeong, K.; Kim, S. Structural response of submerged floating tunnels with free-end boundary condition based on an analytical approach. *Appl. Ocean. Res.* **2024**, *143*, 103861. [CrossRef]

21.   Zhang, H.C.; Liu, S.X.; Li, J.X.; Zhang, R.L.; Hao, J. Interactions between Multi-directional Irregular Waves and a Pile Group in a Side-by-side Arrangement: Statistical Analysis. *Coast. Eng.* **2019**, *147*, 115–134. [CrossRef]

22.   Yu, Y.X.; Zhang, N.C. Transverse forces and resultant forces on array of bi-pile in irregular waves. *China Ocean Eng.* **1990**, *4*, 29–41.